J. Chem. Thermodynamics 93 (2016) 404–415

Contents lists available at ScienceDirect

J. Chem. Thermodynamics

journal homepage: www.elsevier.com/locate/jct

Study of the impact of high temperatures and pressures on the equilibrium densities and interfacial tension of the carbon dioxide/water system

Luís M.C. Pereira [a], Antonin Chapoy [a], Rod Burgass [a], Mariana B. Oliveira [b], João A.P. Coutinho [b], Bahman Tohidi [a,*]

[a] Institute of Petroleum Engineering, Heriot-Watt University, EH14 4AS Edinburgh, UK
[b] CICECO – Aveiro Institute of Materials, Department of Chemistry, University of Aveiro, 3810-193 Aveiro, Portugal

ARTICLE INFO

Article history:
Received 23 February 2015
Received in revised form 30 April 2015
Accepted 5 May 2015
Available online 14 May 2015

Keywords:
Water
Carbon dioxide
Saturated densities
Interfacial tensions
CPA EoS
Density gradient theory

ABSTRACT

The development of successful and economical CO_2 geological storage projects requires a precise estimation of the saturated phase densities and interfacial tension of the CO_2/H_2O system. The axisymmetric drop shape analysis (ADSA) method was used for measuring the interfacial tension of this system at temperatures over the range (298 to 469) K and pressures up to 69 MPa. The phase densities, required to determine accurate *IFT* values, were determined by measuring the oscillation period of the equilibrated phases with an Anton Paar densitometer. A correlation to readily determine the density of the CO_2-saturated water phase in the range of interest is proposed and the use of pure compound densities for the calculation of the interfacial tension values discussed.

The Cubic-Plus-Association equation of state (CPA EoS) was used to estimate the phase behaviour pressure and temperature dependence of the system studied with very good results. Bulk phase properties and influence parameters adjusted to pure compounds surface tensions within the density gradient theory (DGT) were used to predict the CO_2/H_2O interfacial tensions with remarkably low deviations from the measured values.

1. Introduction

Mitigating the atmospheric CO_2 concentration is known to be one of the most challenging and compelling endeavours humanity will face in the years to come. One defining stage in the process involves the safe storage of captured CO_2. Among current options, geological storage of CO_2 is considered to be one of the most promising approaches [1,2]. Furthermore, since nearly two-thirds of the original oil in place (OOIP) is left unrecovered in reservoirs at the end of primary recovery and secondary waterfloods, carbon dioxide enhanced oil recovery (CO_2-EOR) and water alternating gas (WAG) methods have attracted interest within oil companies not only as technical and profitable techniques to increase oil recovery efficiency but also as economical and ecological methods to reduce CO_2 emissions [3–5].

Accurate knowledge of the effect of pressure and temperature on the interfacial tension (*IFT*) of the carbon dioxide/water system is, among other thermophysical properties, critical for the safe and economical design of operations and facilities, maximising the storage of carbon dioxide in the narrow pore throats of rocks in deep geological formations such as aquifers and depleted oil reservoirs [6,7]. This property controls, to a large extent, not only the CO_2 storage capacity of the target reservoir, but also the oil recovery factor in a near-miscible injection processes [3].

The injection targets are estimated to be at depths greater than 2000 m where pressures and temperatures can exceed 30 MPa and 373 K [2,6]. At these conditions, pure CO_2 will be in a supercritical state ($T_c \sim 304.13$ K and $P_c \sim 7.38$ MPa) and with densities higher than 662 kg · m^{-3}. Due to its key role in the design of the processes mentioned above, many studies have been conducted on the experimental measurement of the *IFT* of the CO_2/H_2O system during the last two decades [6,8–26]. In most of these studies the pendant drop method has been used to perform these measurements over a wide range of experimental conditions. However, to the best of our knowledge, data available in the literature above $T = 398$ K is still limited to the study of Shariat *et al.* [25].

A brief literature review carried by Georgiadis *et al.* [23] showed that *IFT* values for the CO_2/H_2O system above CO_2 supercritical conditions are scarce and/or contradictory. Amongst all reasons

* Corresponding author. Tel.: +44 (0) 1314513672.
E-mail address: bahman.tohidi@pet.hw.ac.uk (B. Tohidi).

http://dx.doi.org/10.1016/j.jct.2015.05.005
0021-9614/

pointed for these discrepancies, the presence of impurities, which will not be addressed here, and the assumption of pure density for the phases involved stand out as the most important factors. Yaginuma *et al.* [27], Hebach *et al.* [28], Kvamme *et al.* [19], Chiquet *et al.* [6], Bachu and Bennion [21], Tabasinejad *et al.* [29] and Shariat *et al.* [25] measured the densities of the saturated phases with a vibrating-tube and the results showed that the approximation of the water-saturated vapour phase density to that of pure CO_2 [30] is in fact valid for temperatures and pressures up to 473 K and 140 MPa, respectively. However, as demonstrated by Chiquet *et al.* [6], the effect of dissolved CO_2 on the density of the liquid aqueous phase can cause severe underestimation of the *IFT*s close to the density inverse conditions, where the deviations of the real (measured) density difference from that of pure substances are greatest.

The high costs of experimental facilities and the time needed to perform these measurements necessitate the deployment of theoretical tools, which when validated with experimental data, can be used to correlate or even predict interfacial tensions for a broad range of conditions. Numerous approaches have been proposed in the past few decades for modelling interfacial tensions including the Parachor method [31,32], the corresponding-states theory [33–35], thermodynamic [36,37] and empirical [38] correlations, molecular simulation [39–45] and the density gradient theory (DGT) [46,47], to name just a few. Among these, the DGT has been thoroughly applied in the prediction of *IFT* values of a wide class of systems and interfaces. Such systems include pure substances and mixtures containing hydrocarbons [48–60], alcohols [61–64], esters [65,66], polymers [67–69], near-critical systems [70–73] and most recently, binary aqueous systems containing common gases such as CO_2, CH_4 and N_2 [39,40,74–77].

The DGT approach considers the free energy density of homogeneous fluid (bulk phase) and the influence parameter of inhomogeneous fluid (interface) to determine the density gradient of components in the system across the interface by minimisation of the Helmholtz energy density and compute interfacial tension values [46]. In general, equations of state (EoSs) are used to estimate the equilibrium properties of the bulk phases and to evaluate the energy across the interface. The influence parameters, although they can be derived from theoretical expressions [71,78], are usually fitted to surface tension data of pure substances.

Accurate prediction of *IFT* values relies on the use of adequate EoSs for the description of both bulk phase compositions and densities. For water containing systems, theoretical based equations of state that explicitly take into account the self- and cross-association interactions between the molecules are the most adequate choice. One of the best known and most successful equations of this kind is the Statistical Associating Fluid Theory equation of state (SAFT EoS) and all its variants. Li *et al.* [74], Lafitte *et al.* [39], Niño-Amézquita *et al.* [75] and Khosharay *et al.* [76,77] coupled the DGT approach with SAFT-based EoSs and successfully described the interfacial properties of the CO_2/H_2O system. Despite obtaining good results, they are still limited to a maximum isotherm at $T = 398$ K [76] and with reduced predictive capabilities, as binary interaction parameters within the DGT framework have been regressed against *IFT* values for a limited temperature range [39,75]. Moreover, Li *et al.* [74] and Khosharay *et al.* [76,77] found that the different versions of SAFT considered were not capable of providing, simultaneously, a satisfactory description of both equilibrium phase compositions and interfacial tension values.

Other association equation of state is the Cubic-Plus-Association [79–81]. With a much simpler theoretical basis, derived from the SRK EoS coupled to the Wertheim first-order perturbation theory, has been shown to be able to describe properly phase equilibria and, when combined with the DGT, the interfacial tensions of systems containing non- and self-associating components. With relevance for this work, Tsivintzelis *et al.* [82] investigated the CPA EoS description of the phase equilibria of CO_2 binary mixtures with water, alcohols, glycols and hydrocarbons and Oliveira *et al.* described [83,84] the high pressure (vapour + liquid) equilibria of several binary CO_2 containing systems, with alkanes, alcohols, esters and acids, carbon disulfide and carbon tetrachloride in a broad range of temperatures and pressures. Coupled with the DGT this equation described the surface tensions of the series *n*-alkanes, *n*-perfluoroalkanes, *n*-alkanols and fatty acid esters, using a linear temperature dependence for the influence parameters or constant values for the heavier compounds of the series [64,65]. The influence parameters established for the pure esters were then used to successfully predict biodiesels surface tensions [66].

The good capability shown by the CPA EoS to describe the phase equilibria of water and CO_2 containing systems and, when coupled with the DGT, the interfacial tensions of chain molecules and their mixtures, was extended in this work to provide an accurate description of both the phase behaviour and interfacial tensions of the challenging system CO_2/H_2O.

This paper focusses on addressing some discrepancies and filling in some experimental gaps found in the literature for the interfacial tensions of the CO_2/H_2O system. First, the saturated phase densities were investigated with a U-shape vibrating-tube densitometer and the results were compared both with literature [19,25,27–29,85] and values of the density of the pure components [30]. Furthermore, a correlation for accurately estimating the density of the CO_2-saturated liquid phase at the experimental conditions was regressed against experimental results. Then, the Asymmetric Drop Shape Analysis (ADSA) method in pendant drops was used for assessing the interfacial tension values of this system at temperatures ranging from (298 to 469) K and pressures up to 69 MPa. Finally, using influence parameters regressed from pure component surface tension data, the (DGT + CPA EoS) prediction results were compared against the experimental values with very good results.

2. Experimental

2.1. Materials

The specification and sources of the chemicals used in this work are summarised in table 1. The water used has better specifications than double-distilled water (electrical conductivity <0.02 $\mu S \cdot cm^{-1}$ at $T = 298$ K) and it was degassed by means of an ultra-sonic bath, for 30 min, before commencing each experiment. Toluene and *n*-heptane were used in this work for cleaning purpose only.

TABLE 1
Suppliers and specification of the materials used in this study.

Chemical name	Supplier	Mass fraction purity	Chemical analysis Concentration/10^{-6}
Carbon dioxide	BOC	0.99995	
Toluene	Fischer Scientific	>0.995	
n-Heptane	RathBurn Chemicals	>0.99	
Water	Sigma–Aldrich		$\leqslant$0.01 ppm silicate $\leqslant$0.4 ppm Cl^- $\leqslant$0.4 ppm NO_3^- $\leqslant$1.0 ppm PO_4^{3-} $\leqslant$1.0 ppm SO_4^{2-} $\leqslant$0.01 ppm heavy metals (as Pb)

2.2. Apparatus

The Pendant Drop apparatus used in this work is similar in design to the setup used by Georgiadis *et al.* [23,86–88] and it is depicted in figure 1. The apparatus consists of a custom-designed high-pressure cylinder made of hastelloy HC-276 with an internal volume of 23 cm^3, 4 fluid ports equally distributed around the cell and closed at both ends by two sapphire windows.

The cell temperature is controlled by means of an electrical heating jacket connected to a controller capable of regulating the temperature of the cell with a stability of ±0.1 K. The temperature inside the cell is measured by a high precision PRT probe inserted in the cell, which is long enough to ensure direct contact with the fluids. The pressure is measured by a piezo resistive silicon pressure transducer (Druck PDCR 4060) connected directly to the cell. The temperature and pressure probe are regularly calibrated against a Prema 3040 precision thermometer and a dead weight pressure balance, respectively. This calibration procedure ensures standard uncertainties of $u(P) = 0.04$ MPa and $u(T) = 0.1$ K.

Pure CO_2 is stored in a 300 cm^3 sample piston connected to the cell by means of high pressure tubing and the backpressure in the piston is kept by means of pressurised hydraulic fluid and an automatic high pressure positive displacement DBR pump. Degassed H_2O is transferred from a glass container (H_2O tank) into a 15 cm^3 hand pump (Sitec, model 710.4340) and connected to the valve V_1, located at the top of the cell.

Water drops are created inside the cell at the tip of a stainless-steel capillary tube (o.d. 1.610 ± 0.001 mm) and maintained at equilibrium in contact with the CO_2 phase. Live images of the drops are magnified and displayed on a computer screen by means of a USB camera and magnification lenses. A white LED light source (Euromex, model LE.5211) and a diffusion filter are used to adjust the contrast of the images. The ADSA method [89,90] implemented in the commercial software SCA 20 (Data Physics, Germany) is then used to determine the interfacial tension from the digitalized images. Accordingly, interfacial tension values are calculated by:

$$\gamma = \frac{\Delta\rho g}{(Bk_{apex})^2}, \tag{1}$$

where $\Delta\rho$ is the density difference between the equilibrated phases, g is the gravitational acceleration (9.81 $m \cdot s^{-1}$) and B and k_{apex} are parameters determined from the Laplace equation adjusted to the shape of the pendant drop [89,90]. Additional details concerning to the pedant drop method can be found in the work of Georgiadis *et al.* [23].

From equation (1), the density difference between the equilibrated phases is required for the determination of pertinent *IFT* values. Hence, the densities of the saturated phases were measured separately using the experimental setup illustrated in figure 2 for several isotherms of interest.

The setup consists of a 500 cm^3 equilibrium cell connected to a *HPHT* U-shape vibrating-tube densitometer (Anton Paar, model DMA HPM) with an built-in temperature sensor with a certified standard uncertainty $u(T) = 0.1$ K. The period of vibration is displayed in an evaluation unit (Anton Paar, model mPDS 5) connected to the densitometer. The densitometer and the equilibrium cell are housed in an oven (Cincinnati Sub-Zero, model Z-16), which allows an overall temperature control stability of ±0.1 K. Pressure readings are performed with a piezo resistive pressure transducer (Druck PDCR 4060) with an estimated standard uncertainty $u(P) = 0.04$ MPa. Pure H_2O and CO_2 are stored in two 300 cm^3 sample pistons connected to the top of the equilibrium cell and the backpressure regulated with an automatic high pressure positive displacement DBR pump.

2.3. Experimental procedure

Each piece of the Pendant Drop apparatus including glassware, hand pump, sample cylinders and high-pressure cell were extensively cleaned by using alternately toluene and *n*-heptane. After being drained, deionised water was circulated through all components and the system was dried with compressed air. Once the entire apparatus had been tested for leaks, it was placed under vacuum at a moderate temperature of 333 K. This procedure was repeated before loading the system and helped minimise the presence of impurities during experimental measurements. The desired temperature was set and let to stabilize overnight.

The view cell was filled with CO_2 through the bottom valve and the desire pressure set by means of the hydraulic pump connected to the CO_2 sample cylinder, as depicted in figure 1. Before the start of experiments, water was introduced inside the view cell until a liquid phase was visible on the bottom of the cell and the system was left to reach equilibrium, *i.e.* for the CO_2-bulk phase to be saturated with H_2O. Thereafter, drops were created by opening the top valve and turning the hand pump. For each pressure/temperature state, valves V_1 and V_2 were kept closed and a minimum of 3 consecutive drops were

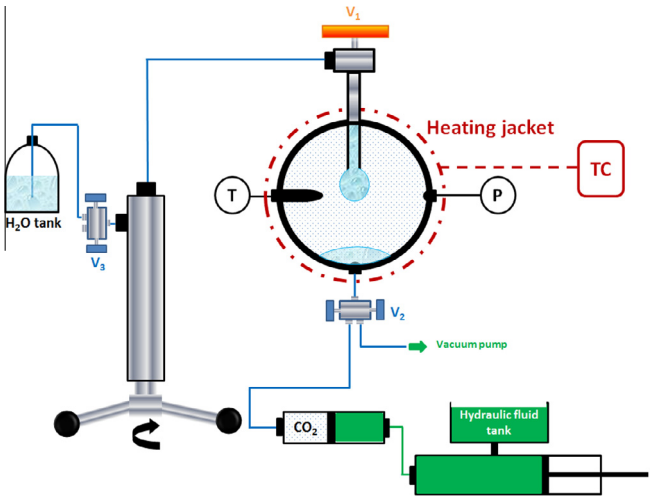

FIGURE 1. Illustrative scheme of the pendant drop setup.

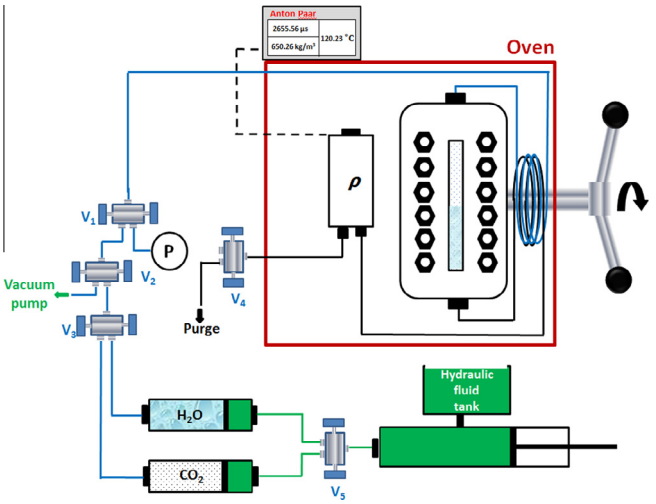

FIGURE 2. Illustrative scheme of the density measuring setup.

recorded during at least 900 s and the software was set to capture pictures every 10 s. The *IFT* data point was obtained by taking the average value calculated from pictures taken within the 300th and 600th second. According to mass transfer models [23] and experimental observation this interval is sufficient for the system to reach equilibrium by diffusion mechanisms alone and to obtain a steady value for the *IFT*. As an example, the *IFT* dependence with time for the isotherms at $T = (298, 374$ and $469)$ K is depicted in figure 3.

The saturated/bulk phase densities were measured by loading the binary mixture into the thermostated equilibrium cell from the CO_2 and H_2O sample pistons, as depicted in figure 2. The desired pressure was set by controlling the amount of fluids injected. The density values of the CO_2-saturated liquid were determined by purging the mixture at constant pressure and flowing this phase through the densitometer. A magnetic stirrer positioned at the bottom of the cell together with a high ratio of volume of system to volume of purge ($V_{system}/V_{purge} \approx 500\ cm^3/2.2\ cm^3$) helped to ensure that equilibrium conditions were maintained throughout measurements. The water-saturated CO_2 phase was also studied by turning the equilibrium cell vertically and repeating the procedure described above.

The measured period of vibration (τ) of a *U* tube can be related to the density (ρ) according to:

$$\rho = D_1\tau^2 - D_2, \tag{2}$$

where D_1 and D_2 are the temperature and pressure dependent densitometer parameters. In our calibration, these parameters were calibrated against pure densities of water and carbon dioxide [30] for each *P*–*T* of interest. To check our calibration procedure and reproducibility, the density of pure H_2O and CO_2 was measured at pertinent conditions and the percentage absolute deviation (*%AAD*) was found to be 0.01% and 0.41%, respectively. Since CO_2 is much more compressible and its density is much more sensitive to temperature and pressure, particularly in the vicinity of the phase transition and critical point, standard uncertainties in pressure ($u(P) = 0.04$ MPa) and temperature ($u(T) = 0.1$ K) can introduce significant variations on the density measurements. Therefore, taking into account all uncertainties and from experimental observation of dispersion of measurements, the estimated combined expanded uncertainties are $U_c(\rho) = 0.7\ kg \cdot m^{-3}$ and $U_c(\rho) = 6.7\ kg \cdot m^{-3}$ for the density measurements in the water and carbon dioxide phases, respectively, with 95% level of confidence within the *P*–*T* range studied.

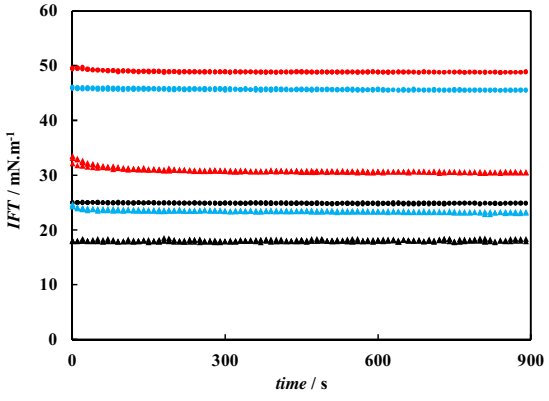

FIGURE 3. *IFT*-time diagram for the CO_2/H_2O system at $T = 298$ K: $P = 3.68$ MPa (●) and $P = 10.63$ MPa (▲); at $T = 374$ K: $P = 5.60$ MPa (●) and $P = 69.12$ MPa (▲) and at $T = 469$ K: $P = 14.91$ MPa (●) and $P = 29.97$ MPa (▲).

3. Model

3.1. Density gradient theory

The density gradient theory (DGT) of fluid interfaces is based on the square gradient theory of van der Waals [47], but only after the reformulation of Cahn and Hilliard [46] it was found useful in modelling interfacial properties. Accordingly, this approach uses statistical thermodynamic-based concepts and phase equilibrium data from bulk phases to estimate the density distribution of each system component across the interface and compute interfacial tension values. Since the DGT has already been presented in great detail in the literature, we refer the reader to previous publications [49,50,52] for a complete description of the model. In summary, by applying the minimisation criterion of the Helmholtz energy to planar interfaces, the interfacial tension values with respects to the density of a reference component is given by [50,52]:

$$IFT = \int_{\rho_{ref}^{I}}^{\rho_{ref}^{II}} \left(2\Delta\Omega(\rho)\sum_i\sum_j c_{ij}\frac{d\rho_i}{d\rho_{ref}}\frac{d\rho_j}{d\rho_{ref}}\right)^{1/2} d\rho_{ref}, \tag{3}$$

$$\Delta\Omega = f_0(\rho) - \sum_i \rho_i\mu_i + p, \tag{4}$$

where $\Delta\Omega$ is the variation of the grand thermodynamic potential, f_0 is the Helmholtz energy density of the homogeneous fluid at local density ρ, μ_i are the pure component chemical potentials, ρ^{I} and ρ^{II} are the bulk phase densities, subscript *ref* stands for the mixture reference component, c_{ij} is the cross influence parameter and p is the equilibrium pressure. The density profiles for water and carbon dioxide across the interface have been solved by applying the methodology described by Li *et al.* [74].

The cross influence parameters are related to pure components influence parameters (c_{ii} and c_{jj}) by:

$$c_{ij} = (1 - \beta_{ij})\sqrt{c_{ii}c_{jj}}, \tag{5}$$

where β_{ij} is the binary interaction coefficient, which has been set here equal to zero making the calculation of interfacial tensions of binary systems fully predictive.

3.2. Phase equilibrium model

The procedure for modelling interfacial tensions first requires the calculation of the equilibrium properties of the two phases separated by the interface being considered at a given temperature and pressure. These calculations were carried out by applying the criterion of equality of the chemical potentials of each component in the coexisting equilibrium phases [91] in combination with the CPA EoS [79,80], using the Soave–Redlich–Kwong cubic term and the conventional van der Waals one fluid mixing rules. This model was also used to evaluate $\Delta\Omega$ (equation (4)) from fundamental thermodynamic relationships [64,92].

The CPA EoS has been extensively applied in the literature to model the phase behaviour of various associating systems [81,84,93–97] and has been shown to be able to provide a correct description of the system under investigation over a wide range of experimental conditions [82,98]. Although CO_2 can be regarded as a non-associating compound, the findings of Tsivintzelis *et al.* [82] revealed the importance of taking into consideration the specific strong interactions between CO_2 and water, mainly Lewis electron (donor + acceptor) type. The best description is obtained when the interactions are accounted for through the procedure proposed by Folas *et al.* [99], where the solvation is taken into account via the modified combining rule CR-1, where the cross-association energy is taken as half of the water self-associating association energy and the cross-association volume is regressed from equilibria

experimental data along with the binary interaction parameter, k_{ij}. In this work, the solvation is taken by considering one cross-associating site in the CO_2 molecules and using the parameters regressed against solubility data over the temperature range (298 to 477) K reported in the work of Tsivintzelis *et al.* [82]. Water was modelled with a 4C association scheme (according to the terminology introduced by Huang and Radosz [100]), in which the hydrogen bonding between the hydrogen atoms and the lone pairs of the oxygen are considered.

The CPA parameters used for water and carbon dioxide are given in table 2, along with the calculated percentage absolute average deviation to the saturation properties from correlations in REFPROP [30] over a broad range of reduced temperatures.

3.3. Influence parameters

As stated before, the influence parameter of pure substances can be derived from theoretical expressions. However, their application to real systems can be rather complicated as these require prior calculation of the radial density distribution function of the pure substances in the homogeneous state [71,78]. To overcome this constraint, the parameters are commonly correlated from surface tension (*ST*) data by rewriting equation (3) for a pure substance:

$$c_{ii} = \frac{1}{2}\left[\frac{ST}{\int_{\rho^{vap.}}^{\rho^{liq.}} ((f_0 - \rho\mu + p))^{1/2} d\rho}\right]^2. \tag{6}$$

For practical purposes, several semi-empirical approaches have been developed and various EoS-dependent correlations are reported in the literature [49,64,65,101] for the estimation of the influence parameter. This parameter increases slowly with increasing temperature but rapidly diverges near the critical point [49]. For this reason most approaches have considered this temperature dependency when combining the DGT with several EoSs. Miqueu *et al.* [49] derived a linear correlation for the influence parameter of hydrocarbons, gases and refrigerants as a function of reduced temperatures ($T_r = T/T_c$) when using the PR EoS. Lin *et al.* [101] generalised the influence parameter of a wide number of compounds as function of critical properties, acentric factor and dipole moment based on the PR EoS and SRK EoS. Queimada *et al.* [53] and Oliveira *et al.* [64] combined the DGT with the CPA EoS and developed a quadratic correlation for the influence parameter with reduced temperatures and accurately described the surface tension of water and a series of *n*-alkanes, *n*-perfluoroalkanes and *n*-alkanols for a broad temperature range with global average errors lower than 1%. That work was also extended to several ester compounds and their mixtures (biodiesels) by the same authors [65,66]. Another approach used by several authors [39,40,57,64,74] consists of taking the influence parameter as a constant value, normally calculated from surface tension data far from the critical point. Most recently, the findings of Khosharay and co-workers [76,77,102] revealed that an influence parameter dependence with both the liquid and vapour densities would produce better results [102], in particular for aqueous interfaces [76,77]. Thus, in this work this approach was adopted for the estimation of density gradient theory influence parameters.

Accordingly, the influence parameters of pure substances calculated from equation (6) are regressed against the liquid and vapour densities by [76,77,102]:

$$c_{ii} = \left|\frac{\rho^L - \rho^V}{A_i\rho^V + B_i\rho^L}\right|, \tag{7}$$

where A_i and B_i are the coefficients for component *i*.

For multicomponent systems, the influence parameters of component *i* are calculated from the regressed coefficients (A_i and B_i) and the mole fraction of component *i* in the coexisting bulk phases and are given by:

$$c_{ii} = \left|\frac{\rho^V y_i - \rho^L x_i}{A_i\rho^L x_i + B_i\rho^V y_i}\right|. \tag{8}$$

The values of A_i and B_i for water and carbon dioxide were obtained by fitting equation (7) to the influence parameters calculated from equation (6) using surface tension data from correlations in REFPROP [30]. Two different sets of coefficients were regressed:

- The first set was fitted against surface tension values over a broad range of reduced temperatures, for water $0.45 < T_r < 0.95$ and for carbon dioxide $0.71 < T_r < 0.98$, as done in the works of Khosharay *et al.* [76,77,102].
- For the second set, the water and carbon dioxide influence parameters were considered to be temperature independent, as suggested by several authors [39,40,74,75], and the coefficients fitted against surface tension data at the lowest reduced temperatures. This procedure is here adopted for the first time and this temperature was selected as opposed to the highest to avoid most of the errors that arise from inappropriate prediction of saturated pure densities by the CPA EoS near the critical point, as characteristic of equations of state without the cross-over approach.

The results are listed in table 3 and plotted in figure 4. As can be seen in figure 4, both sets provide a good description of the surface tension of pure components. The lowest deviations are obtained with the coefficients fitted using surface tension values over a broad range of reduced temperatures, as it could be expected, with a *%AAD* of (1.8 and 2.7)% for water and carbon dioxide, respectively. The second approach resulted in describing the surface tension of H_2O and CO_2 with a *%AAD* of (2.3 and 10.7)%, respectively. This deterioration is partly related to the wide range of temperatures considered, but also to the poor description of the saturation properties by the phase equilibrium model near the critical region, in particular for CO_2 as shown by the results reported in table 2. Nonetheless, as it will be shown further in this work, this set allowed the best *IFT* predictions for the binary system studied.

4. Results and discussion

4.1. Equilibrium densities

The measured equilibrium densities values were compared to those of pure components [30] and to selected data available in the literature [19,25,27–29,85] and the results are plotted in figure 5 and listed in tables S1 and S2 in supporting information.

As can be seen in figure 5, for all isotherms the density of the water-saturated CO_2 phase is very close to that of pure CO_2 within the experimental uncertainty. This is also in accordance with what was already ascribed by several authors in the literature [6,19,25,28,29,85] and hence, the density of this phase can be fairly approximated to that of pure CO_2 [30]. On the other hand, the increase in density of the CO_2-saturated water phase with pressure exceeds that of pure water for all isotherms investigated and it is in good agreement with the data gathered from open literature [25,28,29,85]. This increase can be divided into two regions: whether CO_2 is gaseous or liquefied/supercritical. The density increase in the CO_2-saturated liquid is more pronounced when in contact with gaseous CO_2 and moderate for liquefied/supercritical CO_2, and must be associated with the well-known decrease in

TABLE 2
CPA parameters and modelling results for pure CO_2 and water.

	a_0/(J · m³ · mol⁻²)	c_1	b/(10⁻⁵ m³ · mol⁻¹)	ε/(J · mol⁻¹)	β	%AAD[a]			Ref
						$P^{Sa.t}$	$\rho^{liq.}$	$\rho^{vap.}$	
H_2O	0.12277	0.6736	1.45	16655	0.0692	0.7	1.1	2.4	[93]
CO_2	0.35079	0.7602	2.27	–	–	0.3	1.5	4.5	[82]

[a] *%AAD* calculated for H_2O and CO_2 in the reduced temperature range $0.45 < T_r < 0.95$ and $0.71 < T_r < 0.98$, respectively.

TABLE 3
Adjusted coefficients for the density gradient theory influence parameters density dependence in equation (7).

		A_i/(10²⁰ J⁻¹ · m⁻⁵ · mol²)	B_i/(10²⁰ J⁻¹ · m⁻⁵ · mol²)
First set	CO_2	0.3208	0.3315
	H_2O	2.4479	0.5595
Second set	CO_2	1.4589	0.3305
	H_2O	2.3060	0.5707

solubility of CO_2 molecules in the water phase [103]. The deviation between the pure and measured CO_2-saturated water densities is larger at low temperatures and high pressures, with a maximum relative density difference of 1.7% obtained at $T = 298.5$ K and 11.89 MPa.

Despite the overall low relative deviation observed between the pure and CO_2-saturated water densities in figure 5, the density approximation of this phase to that of pure water can result in significantly different overall density difference (*i.e.* $\Delta\rho$) between the two equilibrated fluids for interfacial tension estimations (equation (1)). In particular, this is the case close to the density inversion conditions where the lowest values for $\Delta\rho$ are obtained. As can be seen in figure 5, the approximation of the density of the CO_2-saturated water phase to that of pure water would result in lower values for $\Delta\rho$ and therefore, in an underestimation of the *IFT* values. This behaviour has also been reported by Chiquet *et al.* [6] who estimated a $\Delta\rho$ up to 1.7 times smaller than the one obtained from experiments when pure density assumption for the equilibrated phases is used at $T = 308$ K and 45 MPa.

In this work, a correlation was regressed against values of saturated density of the CO_2-saturated water phase measured here and available in the literature [6,19,25,27,28,85] to estimate the density of this phase at pertinent experimental conditions. The approach proposed by Hebach *et al.* [28] was extended, in this work, to higher temperatures and pressures by using the data over the ranges listed in table 4 and can be described by:

$$\rho_{H_2O}^{Correlation} = a_0 + a_1P + a_2T + a_3P^2 + a_4T^2 + a_5TP + a_6P^3 + a_7T^2P + a_8P^2T, \quad (9)$$

where a_0, a_1, a_2, a_3, a_4, a_5, a_6, a_7, and a_8 are the regressed parameters listed in table 5 and P and T are in MPa and K, respectively. The regression displays a low relative deviation from the experimental values as depicted in figure 6 and ensures calculated densities values for the CO_2-saturated water phase with a quality of reproduction above 99.60% and a *%AAD* of 0.11% in the range studied. The density values of the water-saturated CO_2 phase were assumed to be that of pure CO_2 under the same P and T conditions, without significant loss of accuracy in the estimation of the interfacial tension values. Our density approach allowed a reproduction of the differences in density reported by Kvamme *et al.* [19] at $T = 323$ K with a *%AAD* of 0.15%, confirming to some extend the validity of our method.

4.2. Interfacial tension

The interfacial tension of the CO_2/H_2O system was measured for temperatures ranging from (298 to 469) K and pressures from (0.34 to 69.14) MPa as reported in table 6. Although interfacial tension data for the CO_2/H_2O system are widely available in the literature [6,8–26], only the studies of Park *et al.* [16], Kvamme *et al.* [19], Chiquet *et al.* [6], Bachu and Bennion [21], Chalbaud *et al.* [22], Bikkina *et al.* [24] and Shariat *et al.* [25] have considered the effect of CO_2 dissolution on the density of the aqueous phase and taken the values of density from experiments or models.

The effect of considering pure substance densities [30] in the calculation of the *IFT* values was evaluated and the relative difference to the *true IFT* (*i.e.* considering the density change in the water-rich phase by equation (9)) were calculated by:

$$\Delta IFT_i = IFT_i^{pure} - IFT_i^{true}, \quad (10)$$

and the results plotted in figure 7. As expected, the lower values for the density difference due to the higher density of the CO_2-saturated water phase when compared to the density of pure water, resulted in lower interfacial tension values, as depicted in figure 7 and these are in accordance with the findings of Chiquet *et al.* [6]. This underestimation generally increases with pressure for all isotherms, and the highest underestimations were obtained at the lowest temperatures for constant pressures, with a maximum difference of 7.28 mN · m⁻¹ (*%AAD* of 27.8%) at $T = 333.15$ K and

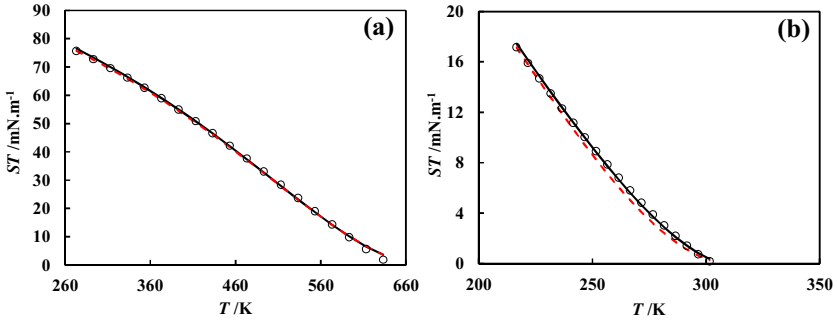

FIGURE 4. *ST*-temperature diagrams for water (a) and carbon dioxide (b). Symbols represent experimental surface tension data obtained from correlations given in REFPROP [30] and lines represent the gradient theory results with influence parameters fitted for an interval of reduced temperatures (solid) and at constant temperature (dashed).

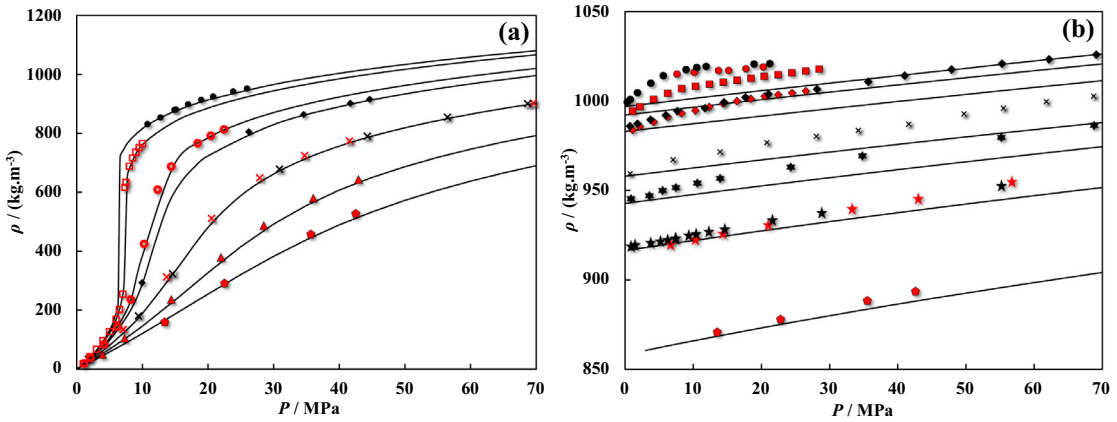

FIGURE 5. (Density + pressure) diagrams of the water-saturated (a) and CO_2-saturated (b) phases of the CO_2/H_2O system. Black symbols represent the experimental data measured in this work: $T = 298$ K (●), $T = 333$ K (♦), $T = 373$ K (×), $T = 393$ K (✱) and $T = 423$ K (★). Red symbols represent literature data: King *et al.* [85], $T = 298$ K (●); Yaginuma *et al.* [27], $T = 304$ K (□); Hebach *et al.* [28], $T = 313$ K (■) and $T = 333$ K (◆); Kvamme *et al.* [19], $T = 323$ K (○); Tabasinejad *et al.* [29], $T = 423$ K (▲); Shariat *et al.* [25], $T = 373$ K (×), $T = 423$ K (★) and $T = 477$ K (⬟). Solid lines represent pure density of CO_2 (a) and water (b) at pertinent temperatures obtained from correlations given in REFPROP [30]. Data from Shariat *et al.* [25] were read from graphs.

TABLE 4
Experimental values used in the regression of equation (9). Results from Shariat *et al.* [25] were read from graphs.

Reference	Pressure/MPa	Temperature/K	Number of data points
King *et al.* [85]	6.6 to 21.8	(293,298)	16
Yaginuma *et al.* [27]	1 to 10.0	304	15
Hebach *et al.* [28]	1.1 to 28.6	(293,313,333)	44
Kvamme *et al.* [19]	1.1 to 22.5	322	11
Chiquet *et al.*[6]	5.0 to 45.0	(308,323,343,363,383)	33
Shariat *et al.* [25]	6.9 to 75.3	(323,422,477)	18
This work	0.73 to 69.1	(298,333,373,393,423)	61
Total			198

59.91 MPa. These conditions also correspond to the lowest calculated density difference $\Delta\rho = 55.8$ kg · m^{-3}, as listed in table 6.

In light of these results, the *IFT* values reported by Hebach *et al.* [14] and Georgiadis *et al.* [23] were recalculated applying the approach followed here for the density difference and the results were plotted against our measurements and the ones from Park *et al.* [16], Chiquet *et al.* [6], Bachu and Bennion [21], Bikkina *et al.* [24] and Shariat *et al.* [25], as depicted in figure 8. The isotherms in the figures are not exactly identical, but sufficiently close for comparison purpose. As can be shown, our measurements are in quite good agreement with data reported by the different authors within the range studied, with the exception of the data reported by Park *et al.* [16], Bikkina *et al.* [24] and Bachu and Bennion [21] at $T = 298$ K figure 8(a), and $T = 313$ K figure 8(b) and $T = 333$ K figure 8(c) where significant deviations are observed in the region where CO_2 is in the liquefied or supercritical state. Overall, the small deviations obtained to the data from Hebach *et al.* [14], Chiquet *et al.* [6], Georgiadis *et al.* [23] and Shariat *et al.* [25] validate both the equipment and methodology adopted, showing these to be capable of accurately determining the *IFT* of this system over a wide range of conditions.

As depicted in figure 8(a) through (c), two regions are distinguishable as the *IFT* decreases with increasing pressures at the three lowest temperatures. Such dependence with pressure has been attributed by different authors [13,23] to the isothermal compressibility of CO_2 and its impact on the Helmholtz energy density. At low pressures, the Helmholtz energy density of CO_2 changes significantly with pressure and therefore the decrease of the interfacial tension values is more pronounced [13]. On the other hand, at high pressures the CO_2-rich phase becomes much less compressible as it reaches a *liquid-like* behaviour and the interfacial tension values decrease gradually [23]. Even though these two regions also appear to be present in the other isotherms studied ($T = 373$, 424 and 469 K), the transition seems to become smoother with increasing temperature. The dependence of the *IFT* on temperature is less marked, with results showing a general decrease of the interfacial

TABLE 5
Regressed coefficients in equation (9).

Coefficient	$\rho^{pure}_{CO_2} \leqslant 467.8$ kg · m^{-3}	$\rho^{pure}_{CO_2} > 467.8$ kg · m^{-3}
a_0/kg · m^{-3}	1025.0	1018.4
a_1/kg · m^{-3} · MPa^{-1}	2.7452	$3.5183 \cdot 10^{-1}$
a_2/kg · m^{-3} · K^{-1}	$3.1077 \cdot 10^{-1}$	$4.4627 \cdot 10^{-1}$
a_3/kg · m^{-3} · MPa^{-2}	$-3.0731 \cdot 10^{-1}$	$2.3878 \cdot 10^{-3}$
a_4/kg · m^{-3} · K^{-2}	$-1.3197 \cdot 10^{-3}$	$-1.5628 \cdot 10^{-3}$
a_5/kg · m^{-3} · MPa^{-1} · K^{-1}	$9.6245 \cdot 10^{-3}$	0
a_6/kg · m^{-3} · MPa^{-3}	$-9.8222 \cdot 10^{-4}$	0
a_7/kg · m^{-3} · MPa^{-1} · K^{-2}	$-3.6286 \cdot 10^{-5}$	0
a_8/kg · m^{-3} · MPa^{-2} · K^{-1}	$7.9860 \cdot 10^{-4}$	0

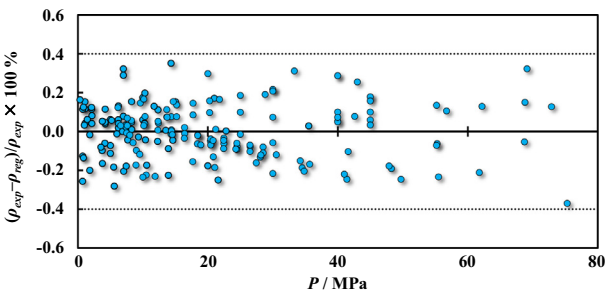

FIGURE 6. Relative deviation between the density of the CO_2-saturated water phase calculated from equation (9) and values from studies listed in table 4.

TABLE 6
Measured interfacial tension data of the CO_2/H_2O system. The density difference used correspond to the difference between the values correlated with equation (9) and pure CO_2 obtained from correlations given in REFPROP [27]. *L*, *G* and *SC* stand for liquid, gaseous and supercritical state, respectively.

T/K	P/MPa	Phase		$\Delta\rho$/(kg · m^{-3})	*IFT*/(mN · m^{-1})	Experimental error/(mN · m^{-1})		
		H_2O	CO_2			U_1	U_2	$U_c = U_1 + U_2$
298.5	0.70	*L*	*G*	989.0	66.95	0.11	0.10	0.21
298.5	1.69	*L*	*G*	971.1	60.56	0.07	0.10	0.17
298.5	3.68	*L*	*G*	924.9	48.70	0.05	0.09	0.14
298.5	5.64	*L*	*G*	847.5	37.74	0.07	0.12	0.19
298.5	6.06	*L*	*G*	817.7	35.06	0.06	0.16	0.22
298.5	6.40	*L*	*G*	779.8	32.97	0.25	0.27	0.52
298.6	6.49[a]	*L*	*G*	765.4	31.69	0.44	0.71	1.15
298.6	6.49[a]	*L*	*L*	310.4	30.79	0.17	1.70	1.87
298.4	6.83	*L*	*L*	283.6	31.00	0.14	0.35	0.49
298.5	7.20	*L*	*L*	268.5	30.99	0.10	0.30	0.40
298.5	8.10	*L*	*L*	239.6	31.09	0.06	0.27	0.33
298.6	8.97	*L*	*L*	220.5	30.98	0.08	0.26	0.34
298.6	10.63	*L*	*L*	192.1	30.73	0.08	0.26	0.34
298.6	13.18	*L*	*L*	161.1	30.62	0.08	0.29	0.37
298.6	15.15	*L*	*L*	142.6	30.81	0.10	0.32	0.42
298.6	20.83	*L*	*L*	103.0	29.84	0.08	0.41	0.49
313.3	0.46	*L*	*G*	986.0	68.52	0.23	0.10	0.33
313.3	1.85	*L*	*G*	962.6	59.60	0.22	0.09	0.31
313.3	3.57	*L*	*G*	927.3	50.67	0.32	0.09	0.41
313.3	5.34	*L*	*G*	878.6	42.75	0.13	0.09	0.22
313.3	7.01	*L*	*G*	806.8	36.65	0.24	0.12	0.36
313.2	9.30	*L*	*SC*	459.7	30.62	0.29	0.53	0.82
313.2	10.44	*L*	*SC*	352.0	29.91	0.32	0.26	0.58
313.3	13.92	*L*	*SC*	249.3	29.59	0.20	0.20	0.40
313.3	20.82	*L*	*SC*	166.4	29.20	0.07	0.25	0.32
313.3	25.68	*L*	*SC*	131.8	28.96	0.10	0.31	0.41
313.3	29.11	*L*	*SC*	112.5	29.05	0.10	0.36	0.46
313.2	31.19	*L*	*SC*	101.9	28.88	0.12	0.39	0.51
333.0	0.92	*L*	*G*	968.8	62.31	0.06	0.09	0.15
333.0	1.79	*L*	*G*	955.1	58.98	0.08	0.09	0.17
333.0	3.66	*L*	*G*	921.3	52.28	0.07	0.09	0.16
333.0	5.00	*L*	*G*	892.2	47.96	0.04	0.09	0.13
333.0	5.85	*L*	*G*	871.0	45.30	0.06	0.09	0.15
333.0	7.18	*L*	*G*	831.7	41.29	0.11	0.09	0.20
333.0	8.89	*L*	*SC*	764.6	36.76	0.10	0.11	0.21
333.1	10.04	*L*	*SC*	703.3	34.08	0.12	0.14	0.26
333.2	11.42	*L*	*SC*	607.6	30.10	0.29	0.17	0.46
333.1	15.01	*L*	*SC*	394.0	29.46	0.19	0.17	0.35
333.2	21.12	*L*	*SC*	261.6	28.13	0.14	0.16	0.30
333.2	24.27	*L*	*SC*	224.6	27.39	0.15	0.18	0.33
333.2	29.58	*L*	*SC*	179.6	27.00	0.14	0.21	0.35
333.2	31.29	*L*	*SC*	167.9	27.25	0.18	0.23	0.41
333.2	39.64	*L*	*SC*	123.0	26.26	0.12	0.29	0.41
333.2	50.31	*L*	*SC*	82.7	26.27	0.11	0.43	0.54
333.2	59.91	*L*	*SC*	55.8	26.16	0.13	0.62	0.75
373.8	0.34	*L*	*G*	952.4	56.79	0.15	0.08	0.23
373.9	1.30	*L*	*G*	939.4	55.02	0.10	0.08	0.18
373.9	3.86	*L*	*G*	901.3	49.03	0.09	0.08	0.17
374.0	5.60	*L*	*G*	871.8	45.62	0.10	0.08	0.18
374.0	7.57	*L*	*SC*	834.1	41.88	0.07	0.08	0.15
374.0	12.09	*L*	*SC*	726.0	34.14	0.11	0.08	0.19
374.0	16.96	*L*	*SC*	580.8	29.00	0.11	0.09	0.20
374.0	25.15	*L*	*SC*	389.6	26.41	0.08	0.10	0.18
373.9	40.03	*L*	*SC*	230.1	24.35	0.12	0.15	0.27
374.0	50.18	*L*	*SC*	172.9	23.64	0.09	0.18	0.27
374.1	62.07	*L*	*SC*	126.7	23.38	0.11	0.25	0.36
374.0	69.12	*L*	*SC*	105.4	23.42	0.06	0.29	0.35
424.4	1.55	*L*	*G*	900.7	46.34	0.07	0.07	0.14
424.4	5.81	*L*	*G*	843.0	40.10	0.09	0.07	0.16
424.4	10.21	*L*	*SC*	776.3	34.60	0.05	0.07	0.12
424.4	16.43	*L*	*SC*	670.0	29.00	0.07	0.06	0.13
424.5	23.83	*L*	*SC*	538.6	25.55	0.08	0.07	0.15
424.6	30.05	*L*	*SC*	450.6	22.82	0.04	0.07	0.11
424.6	39.68	*L*	*SC*	343.3	20.89	0.03	0.08	0.11
424.5	50.11	*L*	*SC*	265.4	19.82	0.15	0.10	0.25
424.6	60.19	*L*	*SC*	211.8	18.83	0.12	0.12	0.24
424.6	69.14	*L*	*SC*	175.8	18.42	0.12	0.14	0.26
469.0	5.90	*L*	*G*	808.0	32.91	0.09	0.06	0.15
469.2	10.08	*L*	*SC*	754.1	28.69	0.10	0.05	0.15

(*continued on next page*)

TABLE 6 (*continued*)

T/K	P/MPa	Phase		$\Delta\rho$/(kg · m^{-3})	IFT/(mN · m^{-1})	Experimental error/(mN · m^{-1})		
		H_2O	CO_2			U_1	U_2	$U_c = U_1 + U_2$
469.1	10.79	*L*	*SC*	744.9	28.49	0.06	0.05	0.11
469.2	14.91	*L*	*SC*	690.1	24.88	0.06	0.05	0.11
469.2	17.70	*L*	*SC*	652.7	23.14	0.05	0.05	0.10
469.2	20.71	*L*	*SC*	612.6	21.82	0.06	0.05	0.11
469.2	29.97	*L*	*SC*	497.1	18.22	0.13	0.05	0.18
469.2	40.06	*L*	*SC*	397.7	15.45	0.09	0.05	0.14
469.2	50.16	*L*	*SC*	318.4	13.84	0.07	0.06	0.13
469.4	59.96	*L*	*SC*	261.0	12.73	0.05	0.07	0.12
469.2	69.09	*L*	*SC*	218.7	12.65	0.10	0.08	0.18

$u(P)$ = 0.04 MPa, $u(T)$ = 0.1 K, $U_c(IFT)$ calculated with a level of confidence of 0.95.
[a] (Vapour + liquid + liquid) point.

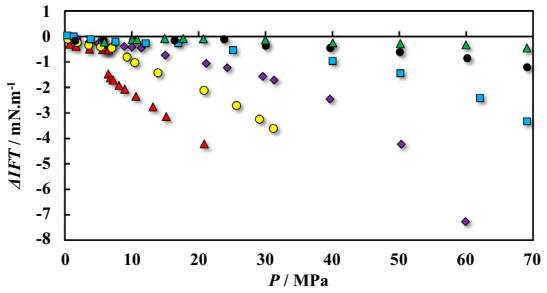

FIGURE 7. Δ*IFT*-pressure diagram of the CO_2/H_2O system for all isotherms studied: T = 298 K (▲), T = 313 K (●), T = 333 K (◆), T = 373 K (■), T = 424 K (●) and T = 469 K (▲).

tension with increasing temperature for temperatures greater than 373 K, and a tendency inversion for lower temperatures, as reported by others [25]. This change must be closely linked with the increase in CO_2 solubility in water as temperature decreases below 373 K [103]. For pressures ranging from about (5 to 15) MPa, the *IFT* values measured at T = (373 and 423) K are similar or greater than the ones measured for lower isotherms, supporting the evidence of the dependence of *IFT* on CO_2 dissolution. Furthermore, as shown in table 6, a point in the (vapour + liquid + liquid) region was observed and three equilibrium phases were present (vapour CO_2, liquid CO_2 and water) at T = 298.6 K and 6.49 MPa. This point is in good agreement with measurements performed by others [104,105]. The interfacial tension values for the vapour CO_2/water and liquid CO_2/water interfaces were found to be (31.69 and 30.79) mN · m^{-1}, respectively, and are in reasonable agreement with the values obtained from MD simulations [43].

The combined expanded uncertainties in the interfacial tension measurements, U_c (*IFT*), are assessed by combining the uncertainties on the drop shape analysis at each recorded image, U_1 (*IFT*), and uncertainties on the estimation of the density difference for the equilibrated phases, U_2 (*IFT*). The first contribution can be estimated to some extent by the standard deviation of the interfacial tension values from the recorded images at each experimental condition. This statistical standard error includes the errors and uncertainties from the use of the Laplace equation, vibrations and reproducibility of the measurements. The effect of uncertainties in pressure and temperature in determining the density of the saturated phases used in the interfacial tension calculations can be evaluated by the law of propagation of errors by [106]:

$$U_2(IFT) = \left(\left(\frac{\partial IFT}{\partial \rho_{H_2O}} \right)^2 U_c(\rho_{H_2O})^2 + \left(\frac{\partial IFT}{\partial \rho_{CO_2}} \right)^2 U_c(\rho_{CO_2})^2 \right)^{1/2}, \quad (11)$$

$$U_c(\rho) = \left(\left(\frac{\partial \rho}{\partial P} \right)^2 u(P)^2 + \left(\frac{\partial \rho}{\partial T} \right)^2 u(T)^2 \right)^{1/2}. \quad (12)$$

The combined expanded uncertainties in the *IFT* measurements estimated with a confidence greater than 95% are shown in table 6 for each experimental condition. It can be observed that in general, the uncertainties caused by the density of the phases are greater than the uncertainties that arise from the ASDA method. The combined expanded uncertainty has an average value of 0.31 mN · m^{-1} and reaches a maximum of 1.87 mN · m^{-1} at the three-phase equilibrium for the *IFT* value between the liquid CO_2 and water phases.

4.3. Modelling

The DGT was coupled with the CPA EoS and their capability to estimate the equilibrium properties and to predict the *IFT* of the CO_2/H_2O system was evaluated by comparison against experimental data measured in the present work and gathered from the literature [107–109], and the results are depicted in figures 9 and 10.

Contrarily to previous works [74,76,77], where binary parameters within the EoS framework were adjusted to both saturated densities and *IFT* data, in this study the CPA EoS binary interaction parameter was taken from the work of Tsivintzelis *et al.* [82] and the *IFT* values were calculated in a fully predictive manner with the DGT, as no β_{ij} different from 0 was used in equation (5). As depicted in figure 9(a), the CPA EoS estimates are in good agreement with experimental solubility over the range of interest and, as can be seen in figure 9(b), it also provided a very good prediction of the pressure and temperature effect on the density difference between the equilibrated phases with a *%AAD* of 5.3%.

As depicted in figure 10(a), the interfacial tension values of the CO_2/H_2O system are severely under predicted with the *first set* of adjusted coefficients for the density gradient theory influence parameters (table 3), this is particularly true at high pressures and low temperatures where CO_2 is either in the liquefied or supercritical state. The model deviations are reduced at high temperatures, resulting in a calculated *%AAD* of 18.2%. On the other hand, by taking the coefficients for the influence parameters adjusted at a fixed temperature (*second set*, table 3), the DGT is able to predict accurately the values of the experimental interfacial tension over all of the temperature and pressure range, with a *%AAD* of 4.5%, as depicted in figure 10(b). It appears that the *IFT* predictions of this system are rather sensitive to the influence parameter of CO_2 as the *second set* leads to influence parameters smaller by one order of magnitude than the ones obtained with the *first set*. Overall, the DGT predictions obtained with the *second set* of coefficients for the CO_2/H_2O system are outstanding, considering the low deviations to measured data obtained for temperatures up to 469 K and pressures up to 69 MPa.

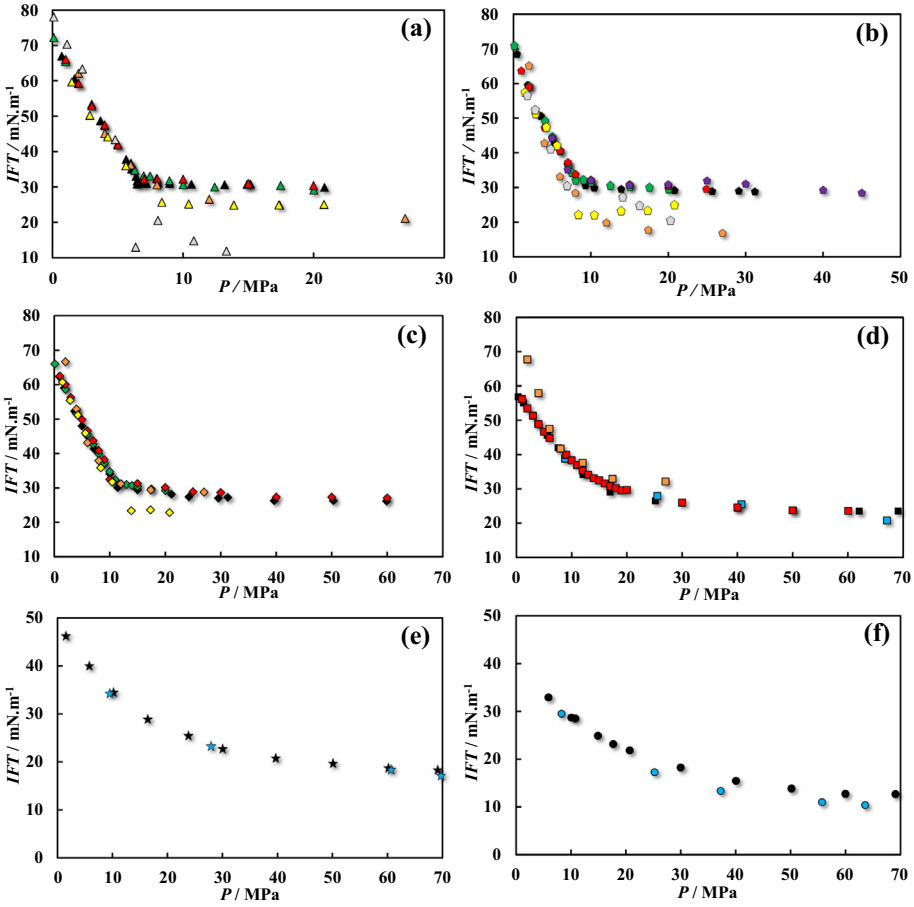

FIGURE 8. *IFT*-pressure diagrams of the CO_2/H_2O system. Full black symbols represent the *IFT* values measured in the present work: $T = 298$ K (▲), $T = 313$ K (⬟), $T = 333$ K (⧫), $T = 374$ K (■), $T = 424$ K (★) and $T = 469$ K (●). Coloured symbols represent literature data: Hebach *et al.* [14], $T = 298$ K (▲), $T = 308$ K (⬟) and $T = 333$ K (◆); Park *et al.* [16], $T = 298$ K (△) and $T = 311$ K (⬠); Chiquet *et al.* [6], $T = 308$ K (⬟); Bachu and Bennion [21], $T = 298$ K (▲), $T = 314$ K (⬟), $T = 333$ K (◆) and $T = 373$ K (■); Georgiadis *et al.* [23], $T = 298$ K (▲), $T = 313$ K (⬟), $T = 333$ K (◆) and $T = 373$ K (■); Bikkina *et al.* [24], $T = 298$ K (△), $T = 313$ K (⬠) and $T = 333$ K (◇); Shariat *et al.* [25], $T = 373$ K (■), $T = 422$ K (★) and $T = 478$ K (●). *IFT* data reported by Hebach *et al.* [14] and Georgiadis *et al.* [23] were recalculated using the correlation developed in this work for estimating the density of the CO_2-saturated water phase. Data from Shariat *et al.* [25] were read from graphs.

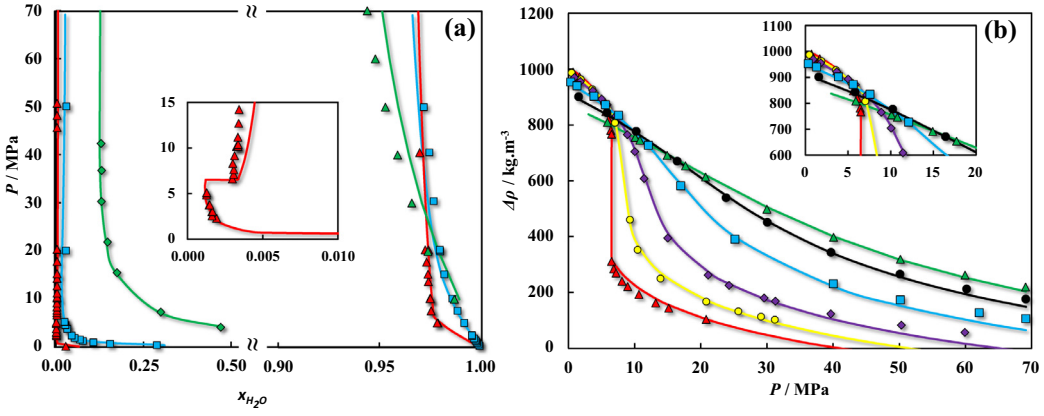

FIGURE 9. Pressure-composition (a) and $\Delta\rho$-pressure (b) diagrams of the CO_2/H_2O system. Symbols in (a) represent solubility taken from the literature: Spycher *et al.* [107], $T = 298$ K (▲) and $T = 373$ K (■); Takenouchi and Kennedy [108], $T = 473$ K (▲); Tabasinejad *et al.* [109], $T = 478$ K (◆). Symbols in (b) represent the density difference used in the calculation of the experimental *IFT* values given in table 6: $T = 298$ K (▲), $T = 313$ K (●), $T = 333$ K (⧫), $T = 373$ K (◆), $T = 424$ K (■) and $T = 469$ K (▲). Solid lines represent the CPA EoS estimates.

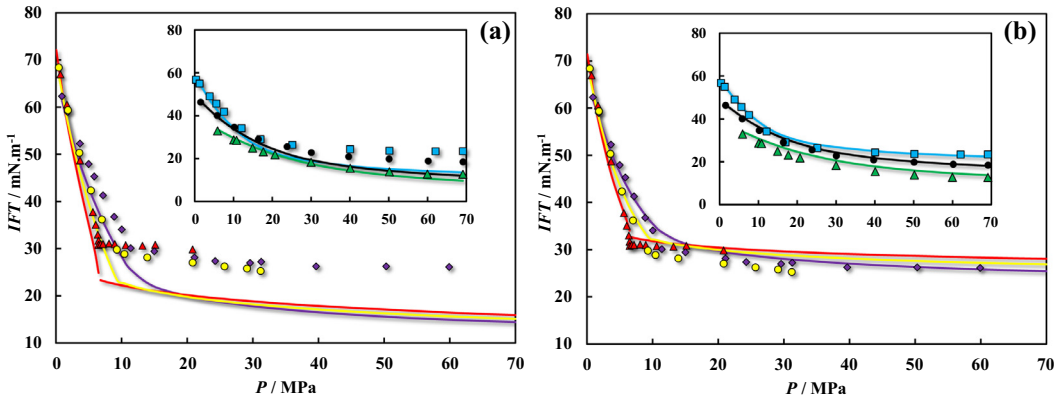

FIGURE 10. *IFT*-pressure diagrams of the CO_2/H_2O system. Symbols represent the *IFT* values measured in the present work: T = 298 K (▲), T = 313 K (●), T = 333 K (◆), T = 373 K (■), T = 424 K (●) and T = 469 K (▲). Solid lines represent the DGT predictions using the *first set* (a) and *second set* (b) of coefficients for the influence parameters of CO_2 and H_2O.

5. Conclusions

Understanding the thermophysical properties of the CO_2/H_2O system over a wide range of temperatures and pressures is essential for the adequate development and optimisation of CO_2 storage in geological formations. In this work, the saturated densities and interfacial tensions of the CO_2/H_2O system were measured over the temperature range (298 to 469) K and pressures ranging from (0.32 to 69.14) MPa, and both the equipment and methodology were validated through comparison against literature data.

The density results show that the approximation of the density of water-saturated CO_2 to that of pure CO_2, as followed by most authors, is in fact valid within the experimental error of measurements. However, CO_2 dissolution in water with increasing pressure lead to density values higher than those of pure water, in particular in the region where CO_2 is in the liquefied or supercritical state. The use of pure component densities for the water phase would, therefore, lead to an underestimation of the *IFT* values, with this being more severe close to the density inversion conditions. In this context the correlation proposed by Hebach *et al.* [28] was readjusted to readily determine the density of the CO_2-saturated water phase in the range of interest and improve the calculation of the *IFT* values.

The coupling of the DGT with the CPA EoS was applied to predict the interfacial tensions of the investigated system. The CPA EoS allowed a good estimation of both experimental solubility and values of the saturated bulk density. Using no more than influence parameters adjusted against surface tension data of the pure compounds at a fixed temperature, the DGT provided a prediction of the measured *IFT* data with a percentage average absolute deviation of 4.5%.

Altogether, novel *IFT* and density measurements for the carbon dioxide/water system were performed at high temperatures and pressures and these results were used to test our modelling approach. Moreover, the very good agreement observed between experimental and modelling results demonstrates the reliability of the experimental values and of the capacity of the predictive method used in this work.

Acknowledgements

This research work is part of an ongoing Joint Industrial Project (JIP) conducted jointly at the Institute of Petroleum Engineering, Heriot-Watt University and the CTP laboratory of MINES ParisTech. The JIPs is supported by Chevron, GALP Energia, Linde AG Engineering Division, OMV, Petroleum Expert, Statoil, TOTAL and National Grid Carbon Ltd, which is gratefully acknowledged. The participation of National Grid Carbon in the JIP was funded by the European Commission's European Energy Programme for Recovery. The authors would also like to thank the members of the steering committee for their fruitful comments and discussions. Luís M.C. Pereira acknowledges the financial support from Galp Energia through his PhD grant. Mariana B. Oliveira acknowledges for her Post-Doctoral grant (SFRH/BPD/71200/2010). JAPC and MBO work was developed in the CICECO-Aveiro Institute of Materials (Ref. FCT UID /CTM/50011/2013), financed by national funds through the FCT/MEC and co-financed by FEDER under the PT2020 Partnership Agreement.

Appendix A. Supplementary data

Supplementary data associated with this article can be found, in the online version, at http://dx.doi.org/10.1016/j.jct.2015.05.005.

References

[1] S. Pacala, R. Socolow, Science 305 (2004) 968–972.
[2] S.J. Altman, B. Aminzadeh, M.T. Balhoff, P.C. Bennett, S.L. Bryant, M.B. Cardenas, et al., J. Phys. Chem. C 118 (2014) 15103–15113.
[3] D.W. Green, G.P. Willhite, Enhanced Oil Recovery, SPE Textbook Series, 1998.
[4] J.R. Christensen, E.H. Stenby, A. Skauge, S.P.E. Reserv, Eval. Eng. 4 (2001) 97–106.
[5] S.H. Talebian, R. Masoudi, I.M. Tan, P.L.J. Zitha, J. Pet. Sci. Eng. 120 (2014) 202–215.
[6] P. Chiquet, J.-L. Daridon, D. Broseta, S. Thibeau, Energy Convers. Manage. 48 (2007) 736–744.
[7] S. Iglauer, C.H. Pentland, A. Busch, Water Resour. Res. 51 (2015) 729–774.
[8] E.W. Hough, G.J. Heuer, J.W. Walker, Pet. Trans. AIME 216 (1959) 469–472.
[9] R. Massoudi, A.D. King, J. Phys. Chem. 78 (1974) 2262–2266.
[10] C. Jho, D. Nealon, S. Shogbola, A.D. King Jr., J. Colloid Interface Sci. 65 (1978) 141–154.
[11] B.-S. Chun, G.T. Wilkinson, Ind. Eng. Chem. Res. 34 (1995) 4371–4377.
[12] A. Wesch, N. Dahmen, K. Ebert, J. Schön, Chem. Ing. Tech. 69 (1997) 942–946.
[13] S.R.P. da Rocha, K.L. Harrison, K.P. Johnston, Langmuir 15 (1999) 419–428.
[14] A. Hebach, A. Oberhof, N. Dahmen, A. Kögel, H. Ederer, E. Dinjus, J. Chem. Eng. Data 47 (2002) 1540–1546.
[15] F. Tewes, F. Boury, J. Phys. Chem. B 108 (2004) 2405–2412.
[16] J.-Y. Park, J.S. Lim, C.H. Yoon, C.H. Lee, K.P. Park, J. Chem. Eng. Data 50 (2005) 299–308.
[17] D. Yang, P. Tontiwachwuthikul, Y. Gu, Energy Fuels 19 (2005) 216–223.
[18] T. Akutsu, Y. Yamaji, H. Yamaguchi, M. Watanabe, R.L. Smith, H. Inomata, Fluid Phase Equilib. 257 (2007) 163–168.
[19] B. Kvamme, T. Kuznetsova, A. Hebach, A. Oberhof, E. Lunde, Comput. Mater. Sci. 38 (2007) 506–513.
[20] Y. Sutjiadi-Sia, P. Jaeger, R. Eggers, J. Supercrit. Fluids 46 (2008) 272–279.
[21] S. Bachu, D.B. Bennion, J. Chem. Eng. Data 54 (2009) 765–775.
[22] C. Chalbaud, M. Robin, J.-M. Lombard, F. Martin, P. Egermann, H. Bertin, Adv. Water Resour. 32 (2009) 98–109.
[23] A. Georgiadis, G. Maitland, J.P.M. Trusler, A. Bismarck, J. Chem. Eng. Data 55 (2010) 4168–4175.

[24] P.K. Bikkina, O. Shoham, R. Uppaluri, J. Chem. Eng. Data 56 (2011) 3725–3733.
[25] A. Shariat, R.G. Moore, S.A. Mehta, K.C. Van Fraassen, K.E. Newsham, J.A. Rushing, Laboratory Measurements of CO2–H2O Interfacial Tension at HP/HT Conditions: Implications for CO2 Sequestration in Deep Aquifers. CMTC 150010-PP presented at Carbon Management Technology Conference held in Orlando, Florida, USA, 7–9 Feb, 2012.
[26] M. Sarmadivaleh, A.Z. Al-Yaseri, S. Iglauer, J. Colloid Interface Sci. 441 (2015) 59–64.
[27] R. Yaginuma, Y. Sato, D. Kodama, Nthon Enerugi Galhzislti 79 (2000) 144–146.
[28] A. Hebach, A. Oberhof, N. Dahmen, J. Chem. Eng. Data 49 (2004) 950–953.
[29] F. Tabasinejad, Y. Barzin, R. Moore, S. Mehta, K. Van Fraassen, J. Rushing, K. Newsham, Water/CO2 System at High Pressure and Temperature Conditions: Measurement and Modeling of Density in Equilibrium Liquid and Vapor Phases. SPE 131636 presented at the SPE EUROPEC/EAGE Annual Conference and Exhibition held in Barcelona, Spain, 14–17 June, 2010.
[30] E.W. Lemmon, M.O. McLinden, M.L. Huber, NIST Reference Fluid Thermodynamic and Transport Properties—REFPROP.v9.0, NIST, Gaithersburg, MD, 2010.
[31] D. Macleod, Trans. Faraday Soc. 2 (1923) 2–5.
[32] C.F. Weinaug, D.L. Katz, Ind. Eng. Chem. 35 (1943) 239–246.
[33] E.A. Guggenheim, J. Chem. Phys. 13 (1945) 253.
[34] Y.-X. Zuo, E.H. Stenby, Can. J. Chem. Eng. 75 (1997) 1130–1137.
[35] A.J. Queimada, L.I. Rolo, A.I. Caço, I.M. Marrucho, E.H. Stenby, J.A.P. Coutinho, Fuel 85 (2006) 874–877.
[36] L.A. Girifalco, R.J. Good, J. Phys. Chem. 61 (1957) 904–909.
[37] P.H. Winterfield, L.E. Scriven, H.T. Davis, AIChE J. 24 (1978) 1010–1014.
[38] R. Sutton, An Improved Model for Water-Hydrocarbon Surface Tension at Reservoir Conditions. SPE 124968 presented at the SPE Anual Technical Conference and Exhibition held in New Orleans, Louisiana, USA, 4–7 October, 2009.
[39] T. Lafitte, B. Mendiboure, M.M. Piñeiro, D. Bessières, C. Miqueu, J. Phys. Chem. B 114 (2010) 11110–11116.
[40] C. Miqueu, J.M. Míguez, M.M. Piñeiro, T. Lafitte, B. Mendiboure, J. Phys. Chem. B 115 (2011) 9618–9625.
[41] L.C. Nielsen, I.C. Bourg, G. Sposito, Geochim. Cosmochim. Acta 81 (2012) 28–38.
[42] X. Li, D.A. Ross, J.P.M. Trusler, G.C. Maitland, E.S. Boek, J. Phys. Chem. B 117 (2013) 5647–5652.
[43] E.A. Müller, A. Mejía, J. Phys. Chem. Lett. 5 (2014) 1267–1271.
[44] J.M. Míguez, J.M. Garrido, F.J. Blas, H. Segura, A. Mejía, M.M. Piñeiro, J. Phys. Chem. C 118 (2014) 24504–24519.
[45] S. Iglauer, M.S. Mathew, F. Bresme, J. Colloid Interface Sci. 386 (2012) 405–414.
[46] J.W. Cahn, J.E. Hilliard, J. Chem. Phys. 28 (1958) 258.
[47] J.S. Rowlinson, J. Stat. Phys. 20 (1979) 197–200.
[48] Y.-X. Zuo, E.H. Stenby, Fluid Phase Equilib. 132 (1997) 139–158.
[49] C. Miqueu, B. Mendiboure, A. Graciaa, J. Lachaise, Fluid Phase Equilib. 207 (2003) 225–246.
[50] C. Miqueu, B. Mendiboure, C. Graciaa, J. Lachaise, Fluid Phase Equilib. 218 (2004) 189–203.
[51] A. Mejía, I. Polishuk, H. Segura, J. Wisniak, Thermochim. Acta 411 (2004) 171–176.
[52] C. Miqueu, B. Mendiboure, A. Graciaa, J. Lachaise, Ind. Eng. Chem. Res. 44 (2005) 3321–3329.
[53] A.J. Queimada, C. Miqueu, I.M. Marrucho, G.M. Kontogeorgis, J.A.P. Coutinho, Fluid Phase Equilib. 228–229 (2005) 479–485.
[54] C. Miqueu, B. Mendiboure, A. Graciaa, J. Lachaise, Fuel 87 (2008) 612–621.
[55] E.A. Müller, A. Mejía, Fluid Phase Equilib. 282 (2009) 68–81.
[56] O.G. Niño Amézquita, S. Enders, P.T. Jaeger, R. Eggers, J. Supercrit. Fluids 55 (2010) 724–734.
[57] O.G. Nino-Amezquita, S. Enders, P.T. Jaeger, R. Eggers, Ind. Eng. Chem. Res. 49 (2010) 592–601.
[58] O. Vilaseca, L.F. Vega, Fluid Phase Equilib. 306 (2011) 4–14.
[59] C. Cumicheo, M. Cartes, H. Segura, E.A. Müller, A. Mejía, Fluid Phase Equilib. 380 (2014) 82–92.
[60] E. Schäfer, G. Sadowski, S. Enders, Fluid Phase Equilib. 362 (2014) 151–162.
[61] P.M.W. Cornelisse, M. Wijtkamp, C.J. Peters, J. de Swaan Arons, Fluid Phase Equilib. 150–151 (1998) 633–640.
[62] H. Kahl, S. Enders, Fluid Phase Equilib. 172 (2000) 27–42.
[63] D. Fu, Ind. Eng. Chem. Res. 46 (2007) 7378–7383.
[64] M.B. Oliveira, I.M. Marrucho, J.A.P. Coutinho, A.J. Queimada, Fluid Phase Equilib. 267 (2008) 83–91.
[65] M.B. Oliveira, J.A.P. Coutinho, A.J. Queimada, Fluid Phase Equilib. 303 (2011) 56–61.
[66] S.V.D. Freitas, M.B. Oliveira, A.J. Queimada, M.J. Pratas, Á.S. Lima, J.A.P. Coutinho, Energy Fuels 25 (2011) 4811–4817.
[67] C.I. Poser, I.C. Sanchez, J. Colloid Interface Sci. 69 (1979) 539–548.
[68] G.T. Dee, B.B. Sauer, J. Colloid Interface Sci. 152 (1992) 85–103.
[69] B.B. Sauer, G.T. Dee, J. Colloid Interface Sci. 162 (1994) 25–35.
[70] S. Fisk, J. Chem. Phys. 50 (1969) 3219.
[71] A.J.M. Yang, P.D. Fleming III, J.H. Gibbs, J. Chem. Phys. 64 (1976) 3732.
[72] M.K. Gupta, R.L. Robinson Jr., SPE Reserv. Eng. (1987) 528–530.
[73] M. Sahimi, B.N. Taylor, J. Chem. Phys. 95 (1991) 6749.
[74] X.-S. Li, J.-M. Liu, D. Fu, Ind. Eng. Chem. Res. 47 (2008) 8911–8917.
[75] G. Niño-Amézquita, D. van Putten, S. Enders, Fluid Phase Equilib. 332 (2012) 40–47.
[76] S. Khosharay, M. Abolala, F. Varaminian, J. Mol. Liq. 198 (2014) 292–298.
[77] S. Khosharay, F. Varaminian, Int. J. Refrig. 47 (2014) 26–35.
[78] V. Bongiorno, L.E. Scriven, H.T. Davis, J. Colloid Interface Sci. 57 (1976) 462–475.
[79] G.M. Kontogeorgis, M.L. Michelsen, G.K. Folas, S. Derawi, N. von Solms, E.H. Stenby, Ind. Eng. Chem. Res. 45 (2006) 4855–4868.
[80] G.M. Kontogeorgis, M.L. Michelsen, G.K. Folas, S. Derawi, N. von Solms, E.H. Stenby, Ind. Eng. Chem. Res. 45 (2006) 4869–4878.
[81] M.B. Oliveira, J.A.P. Coutinho, A.J. Queimada, Fluid Phase Equilib. 258 (2007) 58–66.
[82] I. Tsivintzelis, G.M. Kontogeorgis, M.L. Michelsen, E.H. Stenby, Fluid Phase Equilib. 306 (2011) 38–56.
[83] P.J. Carvalho, A.R. Ferreira, M.B. Oliveira, M. Besnard, M.I. Cabaço, J.A.P. Coutinho, J. Chem. Eng. Data 56 (2011) 2786–2792.
[84] M.B. Oliveira, A.J. Queimada, G.M. Kontogeorgis, J.A.P. Coutinho, J. Supercrit. Fluids 55 (2011) 876–892.
[85] M.B. King, A. Mubarak, J.D. Kim, T.R. Bott, J. Supercrit. Fluids 5 (1992) 296–302.
[86] A. Georgiadis, F. Llovell, A. Bismarck, F.J. Blas, A. Galindo, G.C. Maitland, J.P.M. Trusler, G. Jackson, J. Supercrit. Fluids 55 (2010) 743–754.
[87] A. Georgiadis, G. Maitland, J.P.M. Trusler, A. Bismarck, J. Chem. Eng. Data 56 (2011) 4900–4908.
[88] A. Georgiadis, Interfacial Tension of Aqueous and Hydrocarbon Systems in the Presence of Carbon Dioxide at Elevated Pressures and Temperatures (PhD Thesis), Imperial College London, 2011.
[89] P. Cheng, D. Li, L. Boruvka, Y. Rotenberg, A.W. Neumann, Colloids Surf. 43 (1990) 151–167.
[90] B. Song, J. Springer, J. Colloid Interface Sci. 184 (1996) 64–76.
[91] M.L. Michelsen, J.M. Mollerup, Thermodynamic Models: Fundamentals & Computational Aspects, second ed., Tie-Line Publications, 2007.
[92] K.A.G. Schmidt, G.K. Folas, B. Kvamme, Fluid Phase Equilib. 261 (2007) 230–237.
[93] G.M. Kontogeorgis, I.V. Yakoumis, H. Meijer, E. Hendriks, T. Moorwood, Fluid Phase Equilib. 158–160 (1999) 201–209.
[94] G.M. Kontogeorgis, G.K. Folas, F.R. Leon, M.L. Michelsen, Oil Gas Sci. Technol. 63 (2008) 305–319.
[95] H. Haghighi, A. Chapoy, R. Burgess, B. Tohidi, Fluid Phase Equilib. 276 (2009) 24–30.
[96] A. Chapoy, M. Nazeri, M. Kapateh, R. Burgass, C. Coquelet, B. Tohidi, Int. J. Greenhouse Gas Control 19 (2013) 92–100.
[97] A. Chapoy, R. Burgass, B. Tohidi, I. Alsiyabi, J. Chem. Eng. Data (2014). 141103150628006.
[98] A. Chapoy, H. Haghighi, R. Burgass, B. Tohidi, J. Chem. Thermodyn. 47 (2012) 6–12.
[99] G.K. Folas, G.M. Kontogeorgis, M.L. Michelsen, E.H. Stenby, Ind. Eng. Chem. Res. 45 (2006) 1527–1538.
[100] S.H. Huang, M. Radosz, Ind. Eng. Chem. Res. 29 (1990) 2284–2294.
[101] H. Lin, Y.-Y. Duan, Q. Min, Fluid Phase Equilib. 254 (2007) 75–90.
[102] S. Khosharay, M.S. Mazraeno, F. Varaminian, Int. J. Refrig. 36 (2013) 2223–2232.
[103] L.W. Diamond, N.N. Akinfiev, Fluid Phase Equilib. 208 (2003) 265–290.
[104] A. Valtz, A. Chapoy, C. Coquelet, P. Paricaud, D. Richon, Fluid Phase Equilib. 226 (2004) 333–344.
[105] S.-X. Hou, G.C. Maitland, J.P.M. Trusler, J. Supercrit. Fluids 73 (2013) 87–96.
[106] B.N. Taylor, C.E. Kuyatt, Guidelines for Evaluating and Expressing the Uncertainty of NIST Measurement Results, NIST, Gaithersburg, MD, 1994.
[107] N. Spycher, K. Pruess, J. Ennis-King, Geochim. Cosmochim. Acta 67 (2003) 3015–3031.
[108] S. Takenouchi, G.C. Kennedy, Am. J. Sci. 262 (1964) 1055–1074.
[109] F. Tabasinejad, R.G. Moore, S.A. Mehta, K.C. Van Fraassen, Y. Barzin, J.A. Rushing, K.E. Newsham, Ind. Eng. Chem. Res. 50 (2011) 4029–4041.